ISSN: 2395-1680 (ONLINE)
DOI: 10.21917/ijme.2021.0196

BROADBAND CPW FED POLARIZATION RECONFIGURABLE ANTENNA FOR UNIVERSAL UHF RFID READER

Sateesh Virothu and M. Satya Anuradha

Department of Electronics and Communication Engineering, Andhra University College of Engineering, India

Abstract

In this paper, a compact CPW fed polarization reconfigurable wideband antenna is presented for the application of a universal ultra-high frequency (UHF) radio frequency identification (RFID) antenna. In this work, long-range and random orientation detectability features are incorporated with the inclusion of polarization reconfigurability in the RFID reader antenna. Initially, a circularly polarized antenna is designed, which consists of a square slot embedded with an inverted L-shaped strip line and an F-shaped feeding structure, which is etched on the FR4_epoxy substrate. Secondly, the inclusion of three PIN diodes and an extra strip line connected to the feed structure are used to achieve linear as well as circular polarization. The desired performance is obtained in the whole UHF RFID frequency band (universally adopted range in the UHF band by the different countries) from 840 MHz to 960 MHz. Simulation, as well as experimentation procedures, are applied to obtain the details of the S11, gain, axial ratio, and radiation patterns. The experimented performance metrics are in good agreement with simulation results. The results reveal that axial ratio requirements for linear and circular polarizations are met in the required band of operation with accepTable.gain.

Keywords:

RFID, Polarization Reconfigurable Antenna, CPW Feed, PIN Diodes, UHF Band

1. INTRODUCTION

RFID with CP operation has been extensively used in various applications such as the internet of things (IOT), manufacturing industries, and goods in flow systems. Different countries utilize distinct frequency bands authorized for UHF RFID applications. The frequency ranges for UHF RFID applications are 865–867 MHz in India, 866–869 MHz in Europe, 920–926 MHz in Australia, 902–928 MHz in North America, 908.5–914 MHz in Korea, 840.5–844.5 MHz, and 950–956 MHz in Japan, and 920.5–924.5 MHz in China and so on.

Numerous wideband CPW fed square slot antennas have been discussed in the literature. A CPW fed square slot antenna for broadband applications has been presented. The location, width, and length of the tuning stub are varied to obtain optimal impedance bandwidth of 60% [1]. Further improvement in the impedance bandwidth has been achieved with metallic strips added at the corners of the square slot, with the suitable ratio of the metallic strip in the slot to loading metallic strips [2]. Photonic bandgap structures with square-shaped or cross-shaped structures have been implemented in a loop slot, to suppress harmonic control as well as enhancing the bandwidth [3]. Coplanar waveguide (CPW) feed technique used by antennas exhibit many advantages over basic microstrip antennas, like lower dispersion and radiation loss, broader bandwidth, ease of fabrication using MMIC and conformability made the antennas most prevalent [4].

In several communication systems CP antennas play an important role, which eliminates polarization mismatch for various alignment of equipment, also gives benefits such as resistance to unsuitable weather conditions and the reduction in multipath losses. Due to these features, many CP antennas have been implemented in the previous works. The broadband CP operation is experimentally demonstrated by connecting a T-shaped metallic strip to the ground plane at an angle 900 to the feed line [5]. CP mechanism has been introduced with a square slot, inductively coupled with slots and cuts [6], and a ‘C’ shaped grounded strip with diagonal slots has been implemented [7].

The RFID system comprises of the reader and the tags that contain particular information of the objects they are attached. Electromagnetic waves are used to identify and tracking of objects [8]. Many wideband UHF RFID reader antennas with CP operation have been experimentally discussed in previous publications. In [9], Circular polarization and size reduction are achieved by arranging two asymmetric Koch fractal geometries with the single-probe-feed square radiator. Further, four arrow-shaped slots are introduced in diagonal axes of the square radiator to tune resonant frequency around the UHF range. In [10], a frequency reconfigurable UHF RFID reader antenna has been practically tested, and CP radiation is introduced with two L shaped short patches attached to two L shaped radiating strips using PIN diodes. By applying biasing to PIN diodes, the antenna can radiate CP at the two anticipated frequency bands. The overall UHF RFID frequency range 840-960 MHz has been covered with CP operation by utilizing a square slot and F-shaped feeding structure with, an inserted arc-shaped strip [11], a spur line added along the diagonal to the square slot [12], and a T-shaped strip line and three stubs connected to the ground [13]. A CPW fed circular slot with an L-shaped feeding configuration, and two strip lines of L-shaped are placed in the circular slot connected to the ground plane has been practically investigated to achieve broadband impedance bandwidth in CP operation [14].

Some of the research contributions on polarization reconfigurable antennas have been demonstrated for RFID, Wi-Fi, Wi-MAX, and WLAN applications. Switching PIN diodes in on/off conditions linear, left-hand, and right-hand circular polarization modes are achieved for distinct applications [15-21]. Concentrated emissions in LP antennas provide a higher reader range compared to CP antennas exhibiting the same gain. The CP antennas have shorter ranges because the radiated power is distributed in two planes, and are suitable for applications where the tags are oriented in random directions.

The reader antennas of RFID system designed in the operating band of 840 to 960 MHz would be useful for universal applications, which reduce cost-effectiveness. An RFID reader antenna exhibiting both linear and circular polarization is preferable to cover most of the applications. A CPW fed RFID reader with reconfigurable linear and circular polarizations in the UHF band is not published in earlier works. In the present work, a polarization reconfigurable RFID reader antenna has been investigated. To achieve the desired UHF RFID reader antenna performance, a CPW fed square slot antenna with an F-shaped feeding structure, embedded inverted L-shaped stripline to the ground, three PIN diodes, and an extra strip line connected to the feed are utilized in the proposed antenna design. The design covers the complete UHF RFID range from 840 MHz to 960 MHz.

The rest of the paper is organized with the following sections: section 2 discussed antenna design considerations. In part 3 discussed the simulated and experimental results. Finally, the conclusion is presented in section 4.

2. ANTENNA DESIGN CONSIDERATION

The compact polarization reconfigurable antenna geometry with three PIN diodes (D_1, D_2, and D_3) is illustrated in Fig.1(a). And the fabricated antenna is shown in Fig.1(b). The optimal proposed antenna dimensions are presented in Table.1. The antenna is printed on an FR4_epoxy substrate (ε_r = 4.4, h = 0.8 mm and dielectric loss tangent = 0.02), and its overall dimension is 114×114×0.8 mm^3. Initially, the operating frequency 890 MHz calculated using Eq.(1),

$$f_c = \frac{c}{2\pi\sqrt{\varepsilon_{reff}}}\sqrt{\left[\left(\frac{m\pi}{p}\right)^2 + \left(\frac{n\pi}{q}\right)^2\right]} \quad (1)$$

where c is 3×10^8 m/s, ε_{reff} is the effective permittivity of the substrate, p and q are sizes of the square slot. The dimension of the radiating square slot is 86×86mm^2.

The antenna structure is excited with an F-shaped feeding configuration is depicted in Fig.1. The dimensions L_2 and L_3 contribute TE10 and TE01 modes respectively, CP radiation can be produced with two orthogonal modes of equal magnitude and a phase difference of 900. Incorporating an inverted L-shaped stripline connected to the ground in the square slot, which disturbs surface electric field distribution, and hence, circularly polarized modes are excited. The length L_4 acts as a stub to produce the broader resonating bandwidth. In order to obtain polarization reconfigurability, an extra strip line is embedded to the feed structure using PIN diode D_1, and PIN diodes D_2 and D_3 are placed in an inverted L-shaped strip line.

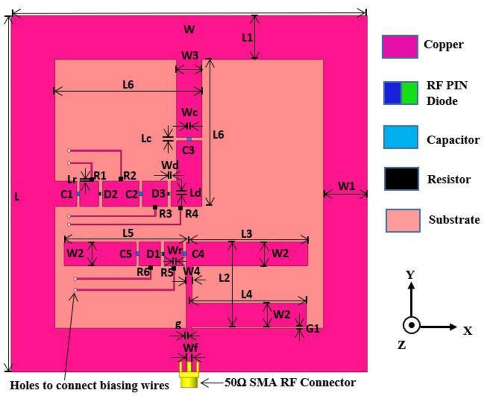

(a)

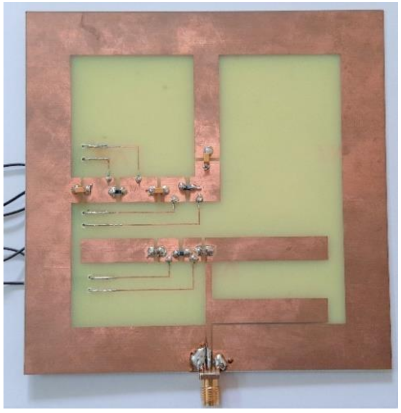

(b)

Fig.1. (a) Detailed dimensions of the designed antenna (b) Fabricated prototype

Applying the biasing voltages to these three PIN diodes, both circular and linear polarized waves can be radiated. Circular polarization can be obtained when D_1 OFF, D_2, and D_3 ON, and linear polarization can be obtained when D_1 ON, D_2, and D_3 OFF. To reduce the effect of external bias voltage on antenna performance, three 10 µF and two 100 µF dc blocking capacitors, and six 3.3 KΩ resistors are used in the configuration. BAR64 series PIN diodes are used for switching action. From the datasheet specifications, in the on-state, the diode exhibits 3.1Ω resistance in series with 1.8 nH inductance, and 1.8 nH inductance in series with the parallel combination of 3.4 KΩ resistance and 0.2 pF capacitance in the off-state as shown in Fig.2.

Table.1. Optimum Antenna Dimensions

Dimension	Value (mm)	Dimension	Value (mm)
W	114	L_5	40
L	114	L_6	47
W_1	14	G	0.4
W_2	7.5	G_1	0.5
W_3	8	Wf	1.48
W_4	2	Ld	1
L_1	14	Wd	1.25
L_2	27	Lc	1
H	0.8	Wc	1.25
L_3	38	Lr	0.5
L_4	39.5	Wr	0.4

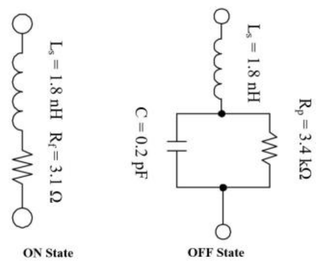

Fig.2. BAR 64-03W PIN diode equivalent circuit

3. RESULTS AND DISCUSSION

3.1. SIMULATION RESULTS

To achieve the universal RFID reader antenna performance, three evolution processes of the proposed reconfigurable antenna are presented in Fig.3. These designs are simulated by using Ansys HFSS software. Fig.4 illustrates simulation results of the reflection coefficient, axial ratio, and gain characteristics. The first evolution (Ant. 1) of the RFID antenna comprises of an F-shaped feeding structure, which exhibits a -10dB impedance bandwidth in the frequency band of 780 MHz to1070 MHz with a percentage impedance BW of 31.35%. This configuration produces poor CP radiation, as can be seen from Fig.3 (c) axial ratio characteristics.

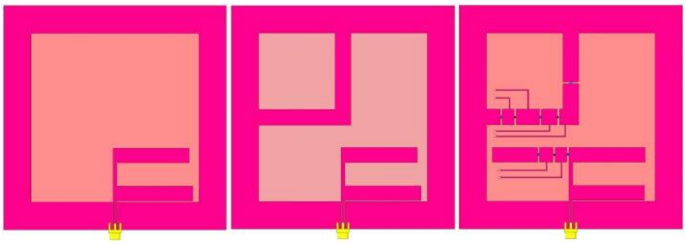

(a) (b) (c)

Fig.3. The geometric evolution of the reconfigurable antenna. (a) Ant.1 (b) Ant. 2 (c) Ant.3 (Proposed)

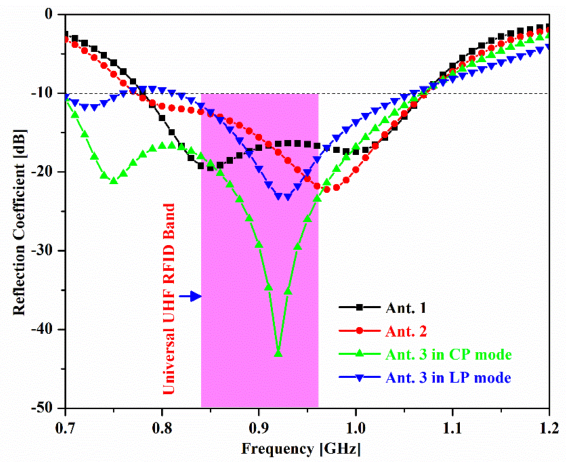

(a)

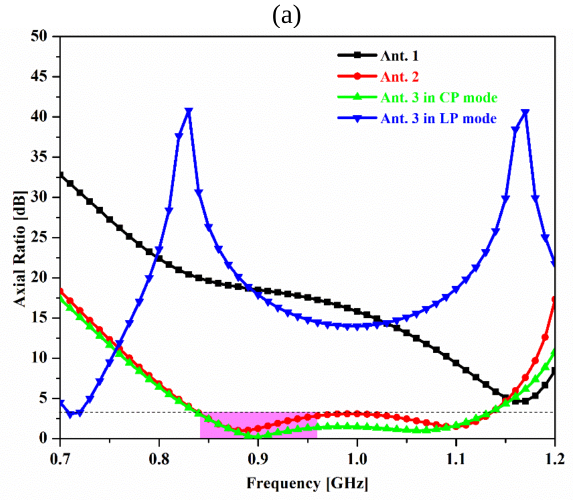

(b)

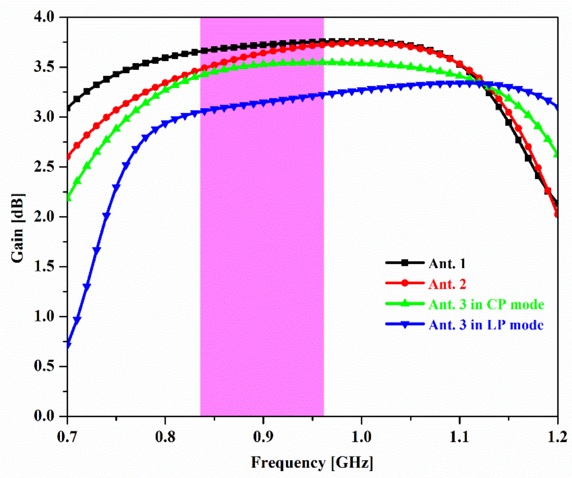

(c)

Fig.4. Simulated plots of designed antenna structures. (a) Reflection Coefficient (b) Axial ratio (c) Gain.

CP radiation is improved in the second evolution process (Ant. 2), an extra inverted L-shaped stripline is placed in the square slot and connected to the ground. This design achieves a -10dB resonating bandwidth of 300 MHz (percentage impedance BW of 32.60%). This design radiates circularly polarized waves having a 3dB axial ratio of 290 MHz in the frequency band of 840 MHz to 1130 MHz.

In the final evolution process (Ant. 3), three PIN diodes and a stripline are incorporated to produce circular as well as linear polarized waves with proper biasing to PIN diodes. This proposed design (Ant. 3) produces circular polarization when D1 OFF, D2, and D3 ON. In this case, the simulated S11 is less than -10dB over the frequency band of 700 to 1070 MHz. It achieves a 3dB axial ratio bandwidth of 290 MHz over a frequency band of 840 MHz to 1130 MHz, with an AR bandwidth (3dB) of 29.44%.

The same antenna structure (Ant. 3) produces linear polarization when D1 ON, D2, and D3 OFF, and provides dual-band -10dB impedance bandwidth in the frequency range of < 700 MHz to760 MHz and 810 MHz to1060 MHz. In the desired band, the percentage impedance BW of 26.7% is obtained and exhibits an axial ratio value of more than 14dB. All the antenna structures radiate with similar gain values except Ant. 3 in LP mode radiates less gain in the required operating band.

Simulated 2D radiation plots are illustrated In Fig.5, and RHCP/LHCP radiation patterns of Ant. 2 and Ant. 3 in CP mode at 890 MHz in the XOZ and YOZ planes are presented in Fig.6. From these figures, it is observed that RHCP and LHCP are radiated along the +z and -z directions, respectively, which shows good symmetry in both directions.

The vector electric field distributions of the proposed Ant. 3 in CP mode at 890 MHz structure for different phase angles (00, 900, 1800, and 2700) are illustrated in Fig.7. These field distributions are observed at a distance of $\lambda_0/4$ from the antenna structure. Electric field vectors at 00 phase angle show that the predominant radiating vectors are in the direction of ‘-x and -y’, for 900, 1800, and 2700 they are directed in ‘-*y* and +x’, ‘+x and +y’, and ‘+y and -x’ respectively. In other words, after each quarter-period, the electric field vectors rotate in the counter clockwise direction by 900 in the +z direction, which explains

RHCP. The same trace is observed for LHCP in the opposite direction.

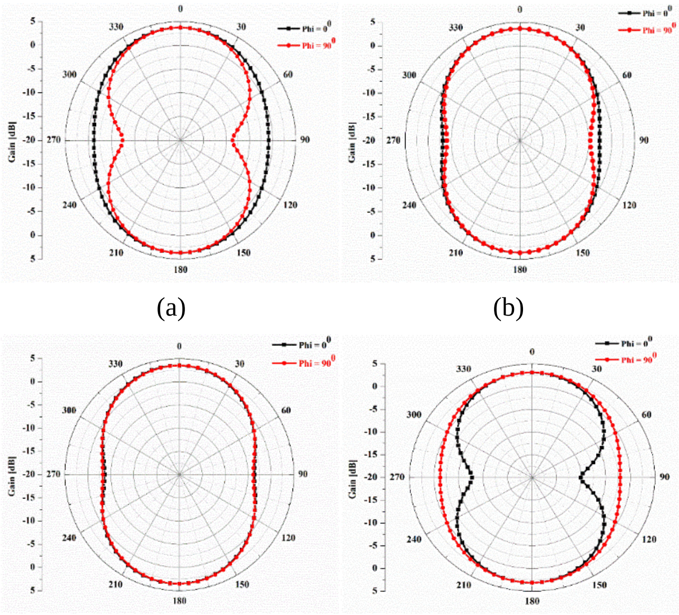

(a) (b) (c) (d)

Fig.5. 2D radiation patterns at 890 MHz in XOZ (Phi = 00) and YOZ (Phi = 900) planes. (a) Ant. 1 (b) Ant. 2 (c) Ant. 3 in CP mode (d) Ant. 3 in LP mode

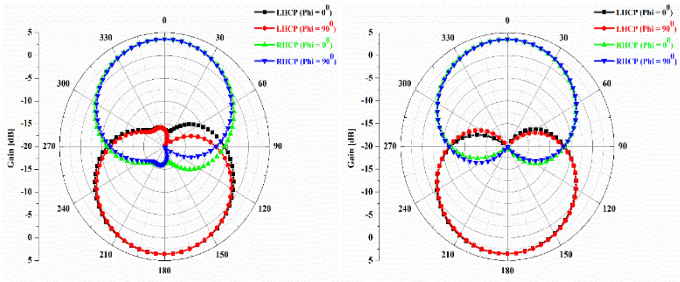

(a) (b)

Fig.6. 2D simulated LHCP/RHCP radiation patterns at 890 MHz in XOZ (Phi = 00) and YOZ (Phi = 900) planes. (a) Ant. 2 (b) Ant. 3 in CP mode.

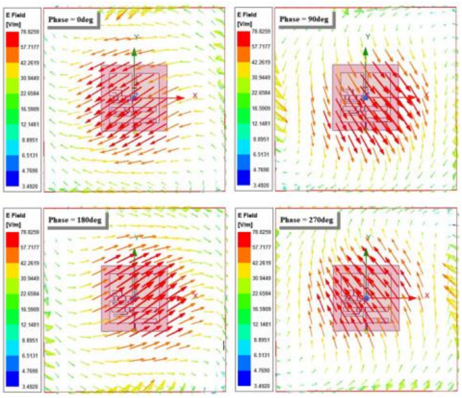

Fig.7. Electric field distribution at a $\lambda_0/4$ distance from proposed antenna in + z direction radiating RHCP for different phase angles (00, 900, 1800, 2700)

3.2. EXPERIMENTAL VALIDATION

The fabricated prototype models were tested for reflection coefficient with a vector network analyzer (VNA) is represented in Fig.8. To obtain the measurement of antenna far-field parameters such as gain, axial ratio, and radiation patterns, the far-field experimental setup is depicted in Fig.9. The measurement setup is arranged in an anechoic chamber with an RF signal generator, spectrum analyzer, two broadband double-ridged horn antennas (DRHA), and a regulator power supply to bias PIN diodes. In the broadside direction, axial ratio and gain are measured.

The Fig.4 and Fig.10 reveals that both simulated and experimented results (S11, axial ratio, and gain) are in good agreement in the universal UHF RFID band. From the measurement results, the -10dB operating bandwidth of Ant. 3 in CP mode is slightly shifted towards the lower frequency end. The measured axial ratio curves related to Ant. 2 and Ant. 3 in both CP and LP modes are represented in Fig.10 (b). In CP mode, the axial ratio value below 3dB is achieved, and in LP mode the axial ratio value is more than 14dB. This reveals that axial ratio requirements for linear and circular polarizations are met in the required band of operation.

(a) (b) (c)

Fig.8. Photographs of vector network analyzers Anritsu MS2037C and Keysight N9914A with measured reflection coefficient. (a) Ant. 2 (b) Ant. 3 in CP mode (c) Ant. 3 LP mode.

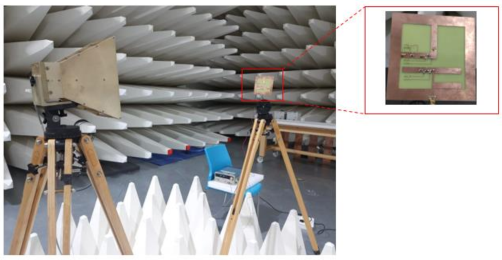

Fig.9. Far-field Measurements set up of proposed polarization reconfigurable antenna to measure axial ratio and gain.

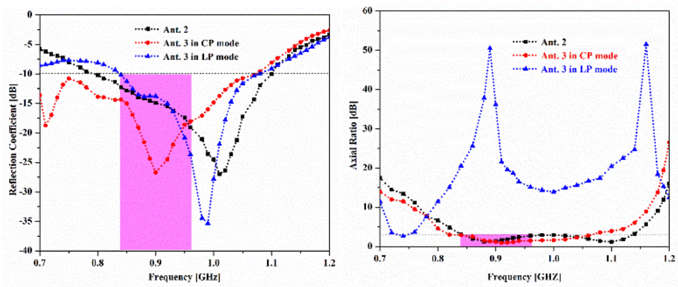

(a) (b)

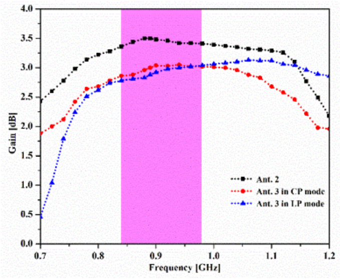

(c)

Fig.10. Measured plots of designed antenna structures. (a) Reflection Coefficient (b) Axial ratio (c) Gain.

For Ant. 3 in CP and LP modes, the measured maximum gain is observed to be 3.03dB and 3.13dB respectively (simulated gain for CP 3.54dB and LP 3.34dB). The reduction in gain values is due to feed connector losses, insertion loss due to PIN diodes, and manufacturing defects.

Although these effects degraded antenna performance, which is tolerable in the operating band and the proposed polarization reconfigurable prototype is well suited for UHF RFID reader applications. The overall simulated and fabrication results are tabulated in Table.2.

The 2D simulated and experimented radiation plots are illustrated in Fig.11, which have been plotted at 890 MHz for considered designs. All the structures radiate symmetrical bidirectional radiation patterns and the 2D radiation measurement plots in XOZ and YOZ planes well-matched with simulated ones.

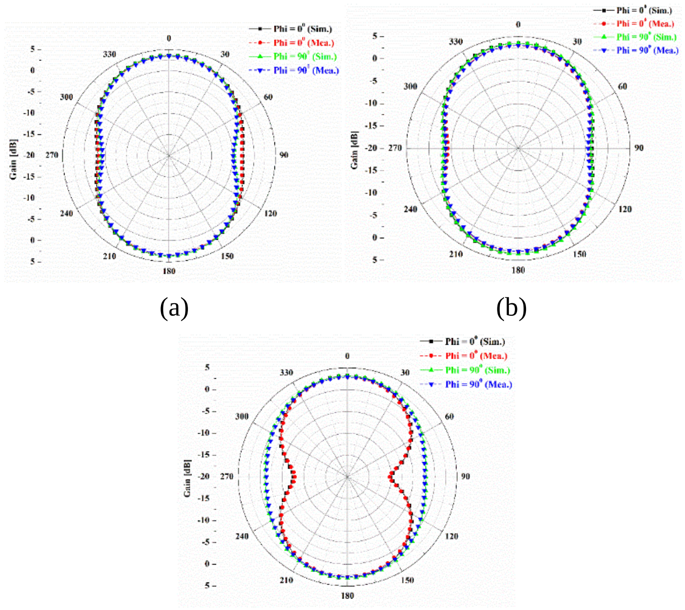

Fig.11. Measured 2D radiation patterns in XOZ and YOZ planes (a) Ant. 2 (b) Ant. 3 in CP mode (c) Ant. 3 in LP mode.

Table.2. Overall simulated and fabricated results

	Ant. 1	**Ant. 2**		**Ant. 3**		**Ant. 3**	
	LP Mode	**CP Mode**		**CP Mode**		**LP Mode**	
	Simulated	**Simulated**	**Measured**	**Simulated**	**Measured**	**Simulated**	**Measured**
f_c (GHz)	0.925	0.92	0.945	0.885	-	- and 0.935	0.949
$S_{11} \leq$ -10 dB f_L - f_H (GHz)	0.78 - 1.07	0.77 - 1.07	0.79 - 1.10	0.7 -1.07	<0.70 - 1.07	<0.70 - 0.76 and 0.81 - 1.06	0.838 - 1.06
Impedance B.W (MHz)/%BW	290/31.35	300/32.60	310/32.8	370/41.80	>370/--	>60/- and 250/26.7	222/23.39
Axial ratio $\leq$ 3 dB f_L - f_H (GHz)	NA	0.84 - 1.13	0.845 - 1.13	0.84 - 1.13	0.825 - 1.07	NA	NA
3 dB Axial ratio BW(MHz)/%BW	NA	290/29.44	285/28.86	290/29.44	245/25.86	NA	NA
Peak gain (dB)	3.75	3.74	3.50	3.54	3.03	3.34	3.13

Table.3. Comparison of proposed RFID antennas with earlier works

Ref. No.		**f_c (MHZ)**	**Impedance (MHz) /%BW**	**3dB Axial ratio BW (MHz) / %BW**	**Gain (dB)**	**Dimensions (mm^3)**
[12]		931	142/15.3	166/17.7	--	126×121×0.8
[13]		886	307/34.6	232/24.3	3.6	114×114×0.8
[14]		870	420/48.3	380/39.4	3.67	114×114×0.8
[15]		808	380/47	332/34.7	3.41	120×120×0.8
Ant. 2		945	310/32.8	285/28.86	3.50	114×114×0.8
Proposed Ant. 3	**CP mode**	--	>370/--	245/25.86	3.03	114×114×0.8
	LP mode	950	221/23.26	NA	3.13	

3.3. COMPARISON OF WIDEBAND UHF RFID READER ANTENNAS

In this section, proposed antenna structures compared with the earlier works [11]-[14], is listed in Table.3. All the antennas in the earlier works produce broadband width and wide CP radiation, which are beneficial when tags are in random orientation. But LP antennas provide higher reader ranges than CP antennas and exhibit good performance in several applications where tags are in the known orientation. By comparing these structures, the proposed Ant. 2 gives comparable impedance and CP bandwidths, compact size, and suitable gains over the desired RFID frequency band. The proposed Ant. 3 radiates both CP and LP waves and offers polarization adaptability in various RFID applications, which is proposed in this communication.

4. CONCLUSION

In this communication, a compact polarization reconfigurable CPW fed UHF RFID reader antenna prototype model is experimentally tested and is well-matched with simulation results in the desired band. The designed antenna gives the desired performance over the UHF RFID band of 840 MHz to 960 MHz and produces both linear as well as circular polarization by biasing the PIN diodes. Hence this design exhibits polarization adaptability in various applications to provide a higher reader range (LP mode) and identification of randomly oriented tags (CP mode). This design achieves good impedance bandwidth, axial ratio, gain, and symmetrical bidirectional radiation characteristics. The maximum measured gain obtained with reconfigurable antenna (Ant. 3) in CP and LP modes is 3.03dB and 3.13dB, respectively. This design is well suitable for worldwide UHF RFID reader antenna applications.

REFERENCES

[1] G. Hantos, D. Flynnand and M.P. Desmulliez, "Built-In Self-Test (BIST) Methods for MEMS: A Review", *Micromachines*, Vol. 12, No. 1, pp. 1-28, 2021.

[2] G. Karthy and P. Sivakumar, "Design of Modified March-C Algorithm and Built-In Self-Test Architecture for Memories", *Publicado en 3C Tecnologia*, Vol. 34, pp. 219-229, 2020.

[3] K. Gopalan and S. Pothiraj, "A Saboteur and Mutant based Built-in Self-Test and Counting Threshold-Based Built-in Self Repairing Mechanism for Memories", *Journal of Ambient Intelligence and Humanized Computing*, Vol. 12, pp. 1-13, 2020.

[4] A.M. Aswin and S. Sankar Ganesh, "Implementation and Validation of Memory Built in Self Test (MBIST) Survey", *International Journal of Mechanical Engineering and Technology*, Vol. 10, No. 3, pp. 153-160,2019.

[5] H. Sreenath and G. Narayanan, "FPGA Implementation of Pseudo Chaos-signal Generator for Secure Communication Systems", *Proceedings of International Conference on Advances in Computing, Communications and Informatics*, pp. 804-807, 2018.

[6] P.K. John, "BIST Architecture for Multiple RAMs in SoC", *Procedia Computer Science*, Vol. 115, pp. 159-165, 2017.

[7] B. Querbach, R. Khanna, S. Puligundla, D. Blankenbeckler, P. Chiang and J. Crop, "Architecture of a Reusable BIST Engine for Detection and Autocorrection of Memory Failures and for IO Debug, Validation, Link Training, and Power Optimization on 14-nm SoC", *IEEE Design and Test*, Vol. 33, No. 1, pp. 59-67, 2016.

[8] B. Mohammad, H. Saleh and M. Ismail, "Design Methodologies for Yield Enhancement and Power Efficiency in SRAM-Based SoCs", *IEEE Transactions on Very Large Scale Integration (VLSI) Systems*, Vol. 23, No. 10, pp. 2054-2064, 2015.

[9] I. Pomeranz, "Computation of Seeds for LFSR-Based Diagnostic Test Generation", *IEEE Transactions on Computer-Aided Design of Integrated Circuits and Systems*, Vol. 34, No. 12, pp. 2004-2012, 2015.

[10] A. Kavitha and S. Sasi Kumar, "A Novel Two-Fold State Skip Logic Built-In Self-Test Scheme for Digital Circuits", *Computers and Electrical Engineering*, Vol. 48, pp. 239-246, 2015.

[11] V. Begam and S. Baulkani, "Ring Counter Based ATPG for Low Transition Test Pattern Generation", *The Scientific World Journal*, Vol. 2015, pp. 1-6, 2015.

[12] S. Vennelakanti and S. Saravanan, "Design and Analysis of Low Power Memory Built in Self-Test Architecture for SoC based Design", *Indian Journal of Science and Technology*, Vol. 8, No. 14, pp.1-5, 2015.

[13] G. Theodorou, N. Kranitis, A. Paschalis and D. Gizopoulos, "Software-Based Self-Test for Small Caches in Microprocessors", *IEEE Transactions on Computer-Aided Design of Integrated Circuits and Systems*, Vol. 33, No. 12, pp. 1991-2004, 2014.

[14] P. Dąbrowski, G. Łabuzek, T. Rachwalik and J. Szmidt, "Searching for Nonlinear Feedback Shift Registers with Parallel Computing", *Information Processing Letters*, Vol. 114, No. 5, pp. 268-272, 2014.

[15] M. Morales-Sandoval, C. Feregrino Uribe, P. Kitsos and R. Cumplido, "Area/Performance Trade-Off Analysis of an FPGA Digit-Serial Montgomery Multiplier based on LFSR", *Computers and Electrical Engineering*, Vol. 39, No. 2, pp. 542-549, 2013.

[16] P. Sakthivel, A. NirmalKumar and T. Mayilsamy, "Low Transition Test Pattern Generator Architecture for Built-in-Self-Test", *American Journal of Applied Sciences*, Vol. 9, No. 9, pp. 1396-1406, 2012.

[17] N. Mukherjee, J. Rajski, G. Mrugalski, A. Pogiel and J. Tyszer, "Ring Generator: An Ultimate Linear Feedback Shift Register", *Computer*, Vol. 44, No. 6, pp. 64-71, 2011.

[18] N. Concer, L. Bononi, M. Soulie, R. Locatelli and L. Carloni, "The Connection-Then-Credit Flow Control Protocol for Heterogeneous Multicore Systems-on-Chip", *IEEE Transactions on Computer-Aided Design of Integrated Circuits and Systems*, Vol. 29, No. 6, pp. 869-882, 2010.

[19] B. Zhou, Y. Ye, Z. Li, J. Zhang, X. Wu and R. Ke, "A Test Set Embedding Approach based on Twisted-Ring Counter with Few Seed", *Integration, the VLSI Journal*, Vol. 43, No. 1, pp. 81-100, 2010.

[20] A. Abu-Issa and S. Quigley, "Bit-Swapping LFSR and Scan-Chain Ordering: A Novel Technique for Peak- and Average-Power Reduction in Scan-Based BIST", *IEEE Transactions*

on Computer-Aided Design of Integrated Circuits and Systems, Vol. 28, No. 5, pp. 755-759, 2009.

[21] Xinhui Zhang, C. Chen and A. Chakravarthy, "Structure Design and Optimization of 2-D LFSR-Based Multisequence Test Generator in Built-In Self-Test", *IEEE Transactions on Instrumentation and Measurement*, Vol. 57, No. 3, pp. 651-663, 2008.

[22] A. Abu-Issa and S. Quigley, "Bit-Swapping LFSR for Low-Power BIST", *Electronics Letters*, Vol. 44, No. 6, pp. 401-403, 2008.

[23] S. Wang, 2007. A BIST TPG for Low Power Dissipation and high Fault Coverage", *IEEE Transactions on Very Large Scale Integration (VLSI) Systems*, Vol. 15, No. 7, pp. 777-789, 2007.

[24] J. Kakade and D. Kagaris, "Minimization of Linear Dependencies Through the Use of Phase Shifters", *IEEE Transactions on Computer-Aided Design of Integrated Circuits and Systems*, Vol. 26, No. 10, pp. 1877-1882, 2007.

[25] Z. Jiang, Y. Zhan, D. Chen and Y. Wang, "Two Methods of Directly Constructing Probabilistic Public-Key Encryption Primitives based on Third-Order LFSR Sequences", *Applied Mathematics and Computation*, Vol. 171, No. 2, pp. 900-911, 2005.

[26] P. Rosinger, B. Al-Hashimi and N. Nicolici, "Dual Multiple-Polynomial LFSR for Low-Power Mixed-Mode BIST", *IEEE Proceedings - Computers and Digital Techniques*, Vol. 150, No. 4, pp. 209-217, 2003.

[27] S. Wang and S. Gupta, "DS-LFSR: A BIST TPG for Low Switching Activity", *IEEE Transactions on Computer-Aided Design of Integrated Circuits and Systems*, Vol. 21, No. 7, pp. 842-851, 2002.

[28] D. Kagaris and S. Tragoudas, "Computational Analysis of Counter-based Schemes for VLSI Test Pattern Generation", *Discrete Applied Mathematics*, Vol. 110, No. 2-3, pp. 227-250, 2001.

[29] T. Sridhar, D. Ho, T. Powell and S. Thatte, "Analysis and Simulation of Parallel Signature Analyzers", *Computers and Mathematics with Applications*, Vol. 13, No. 5-6, pp. 537-545, 1987.